SANDIA REPORT

SAND2014-20600
Unlimited Release
Printed December 2014

Empirically Derived Strength of Residential Roof Structures for Solar Installations

Stephen F. Dwyer, PhD, PE
Alfred Sanchez
Ivan A. Campos
Walter H. Gerstle

Prepared by
Sandia National Laboratories
Albuquerque, New Mexico 87185 and Livermore, California 94550

Sandia National Laboratories is a multi-program laboratory managed and operated by Sandia Corporation, a wholly owned subsidiary of Lockheed Martin Corporation, for the U.S. Department of Energy's National Nuclear Security Administration under contract DE-AC04-94AL85000.

Issued by Sandia National Laboratories, operated for the United States Department of Energy by Sandia Corporation.

Available to DOE and DOE contractors from
U.S. Department of Energy
Office of Scientific and Technical Information
P.O. Box 62
Oak Ridge, TN 37831

Telephone: (865) 576-8401
Facsimile: (865) 576-5728
E-Mail: reports@osti.gov
Online ordering: http://www.osti.gov/scitech

Available to the public from
U.S. Department of Commerce
National Technical Information Service
5301 Shawnee Rd
Alexandria, VA 22312

Telephone: (800) 553-6847
Facsimile: (703) 605-6900
E-Mail: orders@ntis.gov
Online order: http://www.ntis.gov/search

SAND 2014-20600
Unlimited Release
Printed December 2014

Empirically Derived Strength of Residential Roof Structures for Solar Installations

Stephen F. Dwyer, PhD, PE
Geotechnology & Engineering Department
Sandia National Laboratories
P.O. Box 5800
Albuquerque, New Mexico 87185-0706

Alfred Sanchez, Graduate Research Assistant
Department of Civil Engineering
University of New Mexico
Albuquerque, NM 87131

Ivan A. Campos, Graduate Research Assistant
Department of Civil Engineering
University of New Mexico
Albuquerque, NM 87131

Walter H. Gerstle, Professor
Department of Civil Engineering
University of New Mexico
Albuquerque, NM 87131

ABSTRACT

Engineering certification for the installation of solar photovoltaic (PV) modules on wood roofs is often denied because existing wood roofs do not meet structural design codes based on conservative analysis and codes. This work is intended to show that many roofs *are actually sufficiently strong* given the conservatism in codes, documented allowable strengths, roof-structure system effects, and beam composite action produced by joist-sheathing interaction.

This report provides results from a testing program that documents *actual* load-carrying capacity of residential rooftops built to existing building codes. The results reveal that the actual load-carrying capacity of structural members and systems tested are significantly stronger than allowable loads provided by the International Residential Code (IRC 2009) and the national structural code found in Minimum Design Loads for Buildings and Other Structures (ASCE 7-10).

Engineering analysis of residential rooftops typically ignores the system affects and beam composite action in determining rooftop stresses given a potential PV installation. This extreme conservatism combined with conservatism in codes and published allowable stress values for roof building materials (NDS 2012) lead to the perception that well-built homes may not have adequate load bearing capacity to enable a rooftop PV installation. However, based on the test results presented in this report of residential rooftop structural systems, the actual load-bearing capacity is several times higher than published values (NDS 2012).

CONTENTS

FIGURES

TABLES

NOMENCLATURE

ASCE	American Society of Civil Engineers
ASTM	American Society of Testing and Materials
COV	coefficient of variation
FS	factor of safety
IBC	International Building Code
IRC	International Residential Code
NDS	National Design Specification
OSB	oriented strand board
PCA	partial composite action
PV	photovoltaic
PVC	polyvinyl chloride
psf	pound per square foot
SPF	spruce pine fir
TJI	Trus Joist

1. INTRODUCTION

Today's building codes [ASCE 7-10, IBC 2009, and IRC 2009] are conservative, with a hierarchy of factors of safety. Building codes were first developed in the United States in the 1770s by George Washington and Thomas Jefferson to address size and safety issues, primarily at the local level. Cities and/or states would successively increase the level of safety in response to catastrophes such as the Chicago fire in 1871 and the San Francisco earthquake in 1906. Along the way, many code administrations were instituted. It was not until 2000 that most of these independent organizations finally merged to form the International Building Code (IBC). The IBC references key documents and/or bodies of information. For structural loading and compliance, the IBC adopts conservative versions of the American Society of Civil Engineers (ASCE) Committee 7 "Minimum Design Loads for Buildings and Other Structures" requirements [ASCE 7-10]. Although many local jurisdictions still have their own building codes, most of these codes have adopted the IBC for consistency and to save on the cost of maintaining a workforce to develop a more specific local building code. For one- and two-family dwellings, the International Residential Code (IRC) is employed.

A major impediment to installing rooftop solar photovoltaic (PV) systems involves structural-compliance obstacles regarding building codes in the construction permitting process. The city of Madison, Wisconsin, identified the obstacle presented by the construction building-permit process for solar PV as their number one market barrier (Dwyer 2012). Virtually all of the cities involved in the Solar America Cities program agreed that structural concerns created major market barriers in issuing building permits for new solar rooftop installations in their respective cities.

Based upon our experience, as well as input from practicing engineers, solar installers, and building code officials, it is evident that a significant number of existing residential rooftops do not meet the most common current structural code (ASCE 7-10, IBC 2009, and IRC 2009) requirements, even before PV panels are installed, due to the conservatism in the codes and the engineering analysis utilized. This is, in part, due to the conservatism of structural codes, but more so due to the engineering methodology used to evaluate existing roof structures. Customary engineering analysis methods assume that rafters, joists, and trusses act independently to carry rooftop loads. This is an oversimplification; in fact, a roof framing system is a very indeterminate structure. Roof analysis is further complicated because the primary building material is typically wood, which has a wide variety of structural properties depending on its classification, species, condition, use, size, moisture content, and so on. Consequently, engineers tend to be very conservative in their analyses of load-carrying capacity for residential roof structures. This results in a 'perceived' issue rather than a 'real' issue.

This report summarizes test data derived through an extensive testing program. The testing program includes testing of scaled rooftop members and composite structures of varying sizes and geometries to compare their actual load-bearing capacities to those computed according to the IRC [IRC 2009].

2. WORK SCOPE

The research team developed and executed a series of tests to evaluate the structural behavior of common roof structures. The testing program evaluated the most common roof structure types combined with the historical construction practice and material use. Scaled roof structures were tested to failure. This empirical data or 'actual' load-carrying capacity is compared to code-defined 'allowable.' Testing was performed at the structures laboratory in the Civil Engineering Department at the University of New Mexico.

Figure 1. Testing laboratory.

3. PRELIMINARY EXPLORATORY TESTS

Initial testing was exploratory in nature and concentrated on individual wood beams and the potential strength increase given an individual beam by composite or partial composite action offered by the connection of the overlying sheathing to the beam either by nails or glue.

The bulk of the testing then proceeded to scaled roof structure that evaluated the actual strength of a roof system of rafters or trusses. The results were compared to the code-defined allowable loads revealing a significant factor of safety for these scaled roof structures as described in the following sections.

3.1. Point load testing

As a scoping exercise, the team loaded three wood joist and structural sheathing assemblies similar to those commonly used in residential roof systems to failure in a four-point bending test. All of the assemblies consisted of three simply supported 2"×4"×8' hem-fir joists visually graded as studs by the Western Wood Products Association, spaced at 24" on-center. The oriented strand board's (OSB's) strong axis was oriented perpendicular to the longitudinal axis of the joists. Two of the three-joist assemblies had 7/16"×4'×4' OSB panels attached to the top of the joists, as shown in Figure. 2, leaving a 1/8" gap at midspan. One assembly was constructed with nailed joints and the other with glued-and-nailed joints (8 penny [8d] nails at 11.5" spacing, PL 400 Floor and Deck semi-structural adhesive) to connect the OSB panels to the joists. As a control, the third assembly consisted of three joists without sheathing. The support and loading geometry and the resulting cracking patterns for the three tests are shown in Figure. 3. The load was applied using displacement control at a rate of 0.10 in/min.

Figure 2. Photograph of test setup.

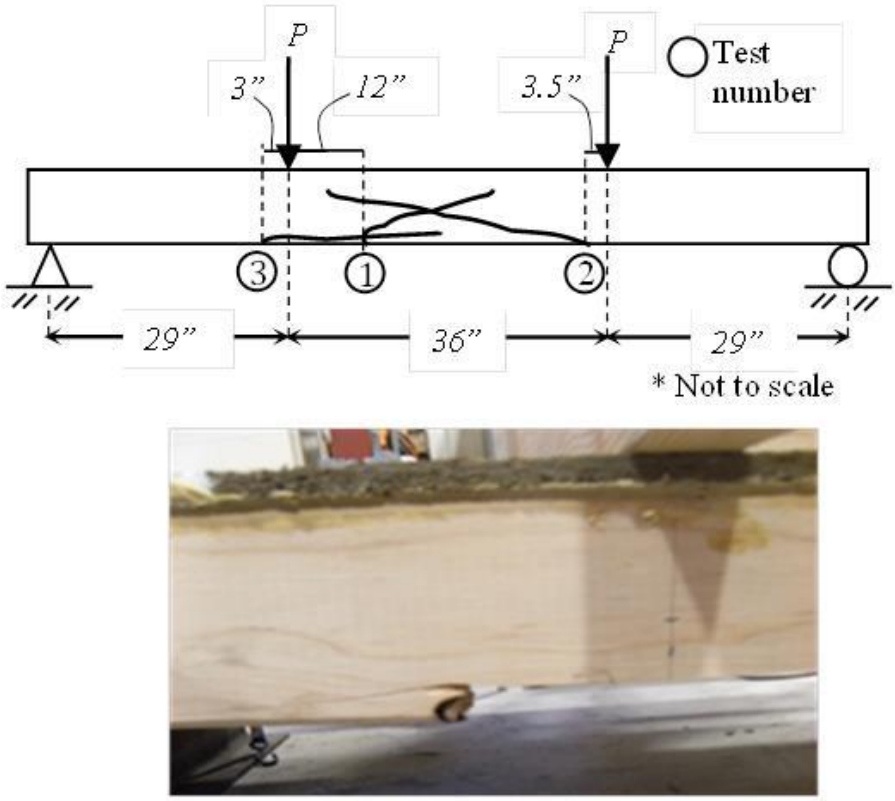

Figure 3. Sketch of cracks in tested joists, and photo of typical crack initiation at knot on tensile face of joist.

In all of the tested assemblies, only one of the three joists failed, perhaps because they were loaded under displacement control. The first joist to fail was always on one side of the assembly. Figure 3 also shows the locations of the cracks that initiated failure in each failed joist (in each case, initiated at the location of a knot on the tensile side of the joist) and their approximate trajectories.

As shown in Figure 4, a load-capacity increase of 73.4% for the glued-and-nailed assembly and a 34.5% increase for the nailed-only assembly, relative to the bare-joist assembly, indicates increased strength for composite assemblies. Nonetheless, this strength increase could be due to the high variability in the bending strengths of the joists themselves, and thus, a larger set of experiments was needed to determine whether this behavior was repeatable.

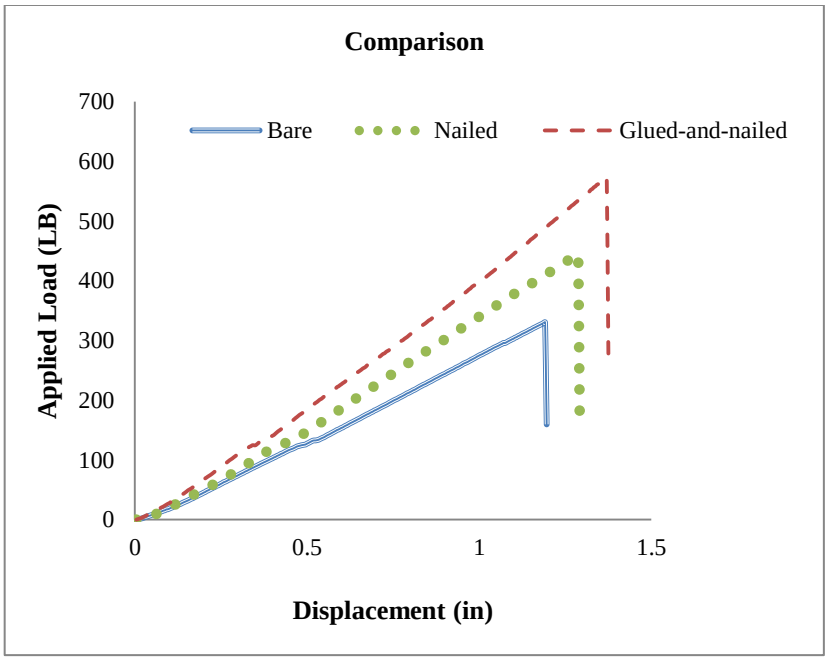

Figure 4. Comparison between loading-displacement relations of preliminary tests.

3.2. Two bare joists, three nailed, and three glued-and-nailed composite joists

Next, the research team performed a set of eight flexural tests to provide more data to better understand the results we obtained in the preliminary tests. These specimens were slightly modified to avoid load-sharing effects and to isolate the effects of composite action between the joist and the OSB. Each specimen consisted of one 2"×4"×8' joist (also visually graded as stud) with two 2'×4', 7/16" OSB panels attached on the top, to form a T- beam (with a 24"-wide flange and the same 1/8" gap at midspan), as shown in Figure 5.

Two bare joists and six composite joists (three with nails and three with nailed-and-glued connections, all on an 11.5" spacing) from a second batch of joists were carefully selected, with variable locations of knots along their spans. The hypothesis tested was that the location of the weakest point in the joist with respect to the location of the gap in the sheathing plays a key role in the effective bending strength of the joist due to partial composite action (PCA). The T-beams and the bare joists were loaded to failure with the same loading conditions as in the preliminary tests, as shown in Figure 5.

Figure 5. Second set test setup.

In this set of experiments, failure of two out of three nailed-only T-beams occurred in a region where a knot existed in the constant-moment region. There was not a knot in the third beam; instead failure initiated at the bottom of the joist three inches away from the gap in sheathing boards, resulting in a higher strength than in the case of joists with knots in the constant-moment region. The load-displacement relation for all specimens demonstrated essentially linear behavior up to failure, as shown in Figure 6, indicating that an increase in stiffness (as the rigidity of the connection at the interface increases) does not necessarily mean an increase in strength. Also, in contrast to the results of the previous set of experiments, the strengths of the glued-and-nailed T-beams were not always higher than the nailed-only T-beams, as shown in Figure 6, although all six of the sheathed joists were stronger than the two bare joists. This variability in strength is attributed to the differing positions and sizes of the strength-controlling knots, among other factors.

Figure 7 shows a 1.5" knot at less than 2" from the gap location in a glued-and-nailed T-beam, resulting in a much lower strength than a nailed-only T-beam. Note that a knot located directly below the gap would be the worst-case scenario in achieving any PCA in the T-beam as the gap plays a major role in the strength of the joist because the flexural stresses at the bottom of the T-beam at this location along the joist are highest.

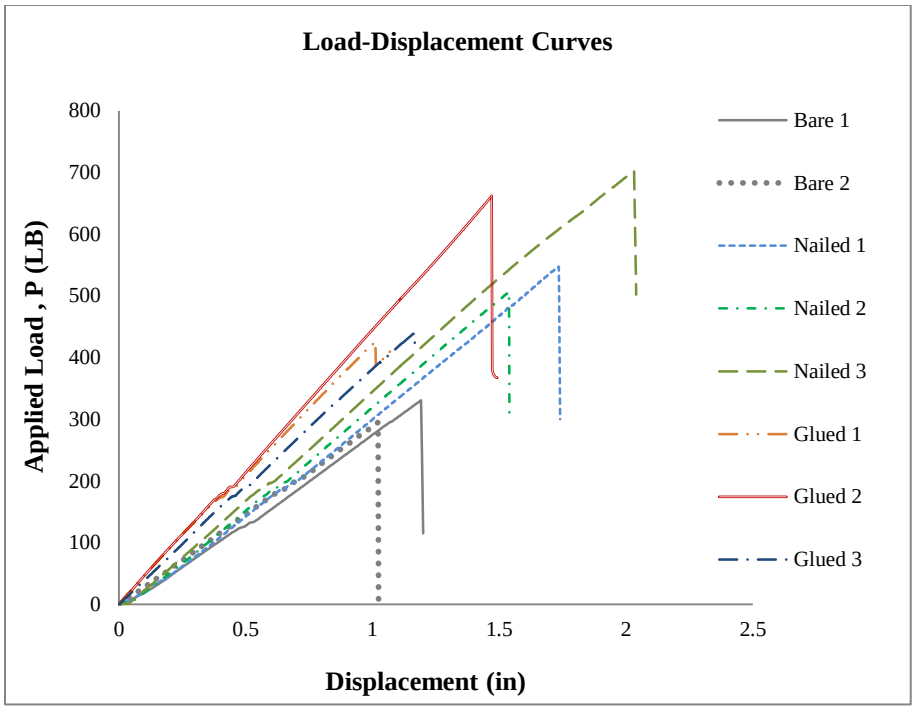

Figure 6. Load-displacement relations for tested specimens.

Figure 7. Knot at almost the same location as gap.

3.3. Nearly identical joists with and without sheathing

The team carefully selected three nominal 4"×4"×8' Douglas-Fir joists visually graded as No. 1, so that knots along the span would go as straight and as perpendicular as possible across a

transverse section of the joist. The purpose was to cut the 4"×4" nominal (3.5"×3.5" actual dimensions) joists into two 2"×4" nominal (1.5"×3.5" actual) joists, as shown in Figure 8, to produce the minimum difference in strength as both joists have nearly identical properties.

Figure 8. Twin 2"×4" joists cut from a single 4"×4" joist.

A four-point bending test was again used, but with a longer 58.5" long constant-moment region. Each of the two 2"×4" joists cut from a single 4"×4" joist were tested separately. As a control, the first 2"×4" joist was tested as a bare joist to obtain the "bare joist strength," while the second 2"×4" joist was tested as the web of a T-beam, as shown in Figure 9, using again two 7/16"×2'×4' OSB panels, and leaving a gap at midspan to obtain the "T-beam strength."

This procedure was designed to illustrate the effect of PCA upon stiffness and strength using two (almost) identical joists. To produce clear behavior, it was decided to glue and nail the interface only between the point loads and the supports of the joist, forcing the slip to occur only at the nails within the constant-moment region (closest to the location of the 0.2"-wide gap). A dial gage was attached to the top of the OSB to measure the gap closure at midspan when the T-beams were loaded.

The bare joist was loaded to failure first. Then the composite T-beam was loaded to the load at which the bare joist had failed and the gap opening was measured. Subsequently, the composite T-beam was loaded to failure. The failure loads, P, for all six of the tested specimens, are shown in Figure 10.

As shown in Figure 10, for each pair of 2"×4" joists, the composite joist was stronger than its noncomposite twin. The load-displacement relations for the twin 2"×4" joists from test No. 1 are shown in Figure 11. An increase in stiffness as well as in strength is evident for the T-beam, compared to the bare joist. The readings from the dial gage at the location of the gap showed that the gap had completely closed when the T-beam reached its bending strength. This closure in the gap means that some continuity of the top flange was present and the OSB began carrying higher compressive forces, and hence, a larger percentage of the total external moment. Note that in all of the previous experiments (with joists with a lower structural grade), the joists failed before the gap could close. The higher the bending strength of the bare joist, the more likely the 1/8" gap is going to close completely, as the T-beam will have a greater curvature and a greater

slip in the nails. The failure of both the bare joist and the T-beam occurred at the same knot in the constant-moment region.

In tests No. 2 and No. 3, the initial gap width was increased to 0.40" to prevent gap closure before failure. The T-beam from test No. 2 registered a total slip of 0.050" on each side of the gap at the failure load of the bare joist, while test No. 3 registered a slip of 0.129" on each side of the gap (the 1/8" gap did not close at these slips). Note, as shown in Figure 10, the strength increase in tests No. 2 and No. 3 (where the gap did not close) is lower than in the previous tests from Set 1 (where lower-strength studs were used).

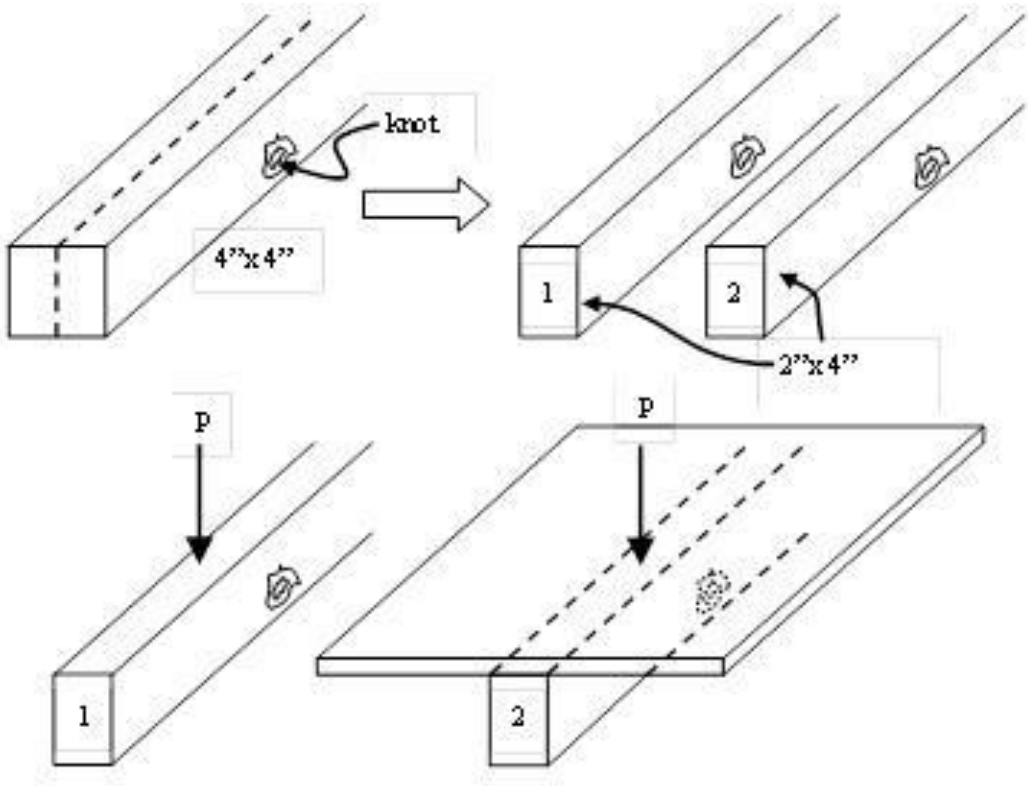

Figure 9. Schematic of the procedure for producing twin joists.

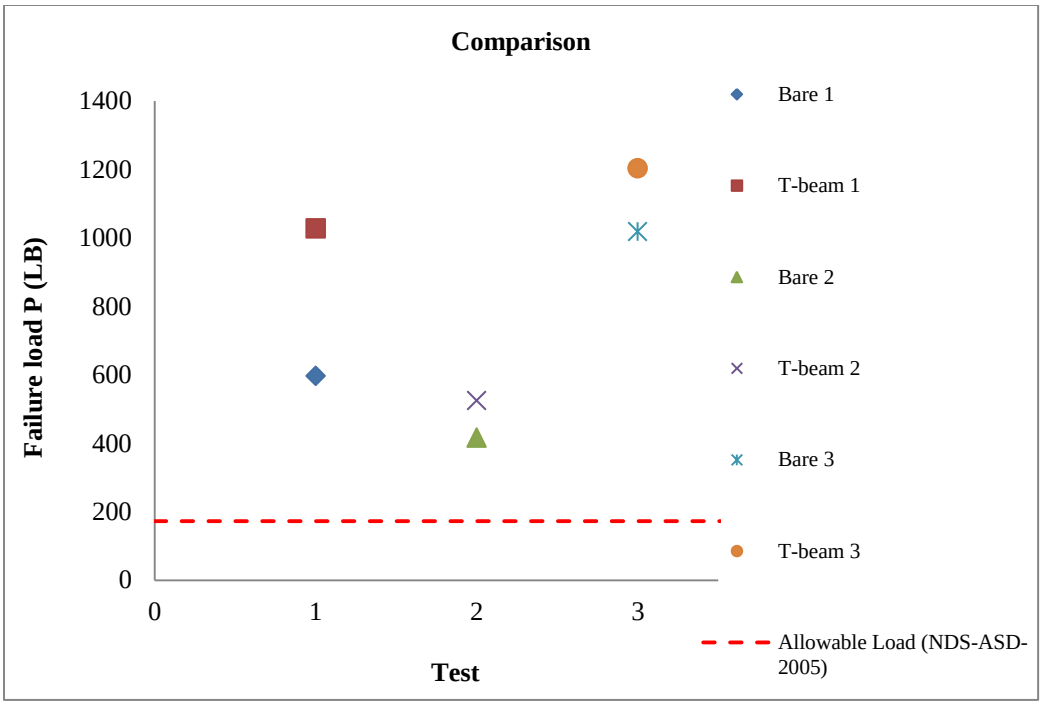

Figure 10. Failure load comparison between specimens.

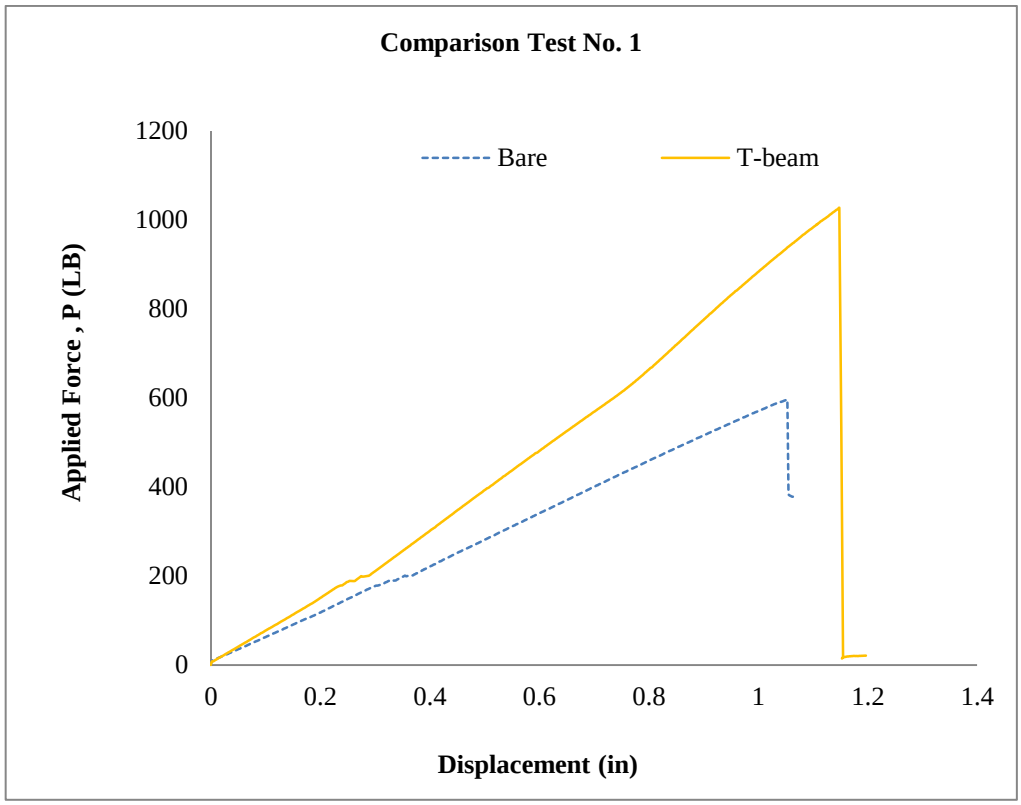

Figure 11. Load-displacement relations for test No. 1.

3.4. Load-displacement properties of nailed joint

Several researchers have tested joist-to-sheathing connections with different specimen configurations and parameters. Mi (2004) tested ten specimens of spruce pine fir (SPF), connected to 7/16" OSB panels with 8d nails, developing a multilinear model for the shear load-shear displacement relation based on his test results. Mi's test setup was used in this research at constant moisture-content conditions, altering only the species of the lumber (Douglas-fir) with almost the same specific gravity as SPF and loading the specimen in compression rather than in tension. A comparison between the resulting load-displacement relations from the test and the multilinear model developed by Mi, for one nail, is shown in Figure 12. As shown in this figure, the newly-obtained relation follows very closely the relation developed by Mi.

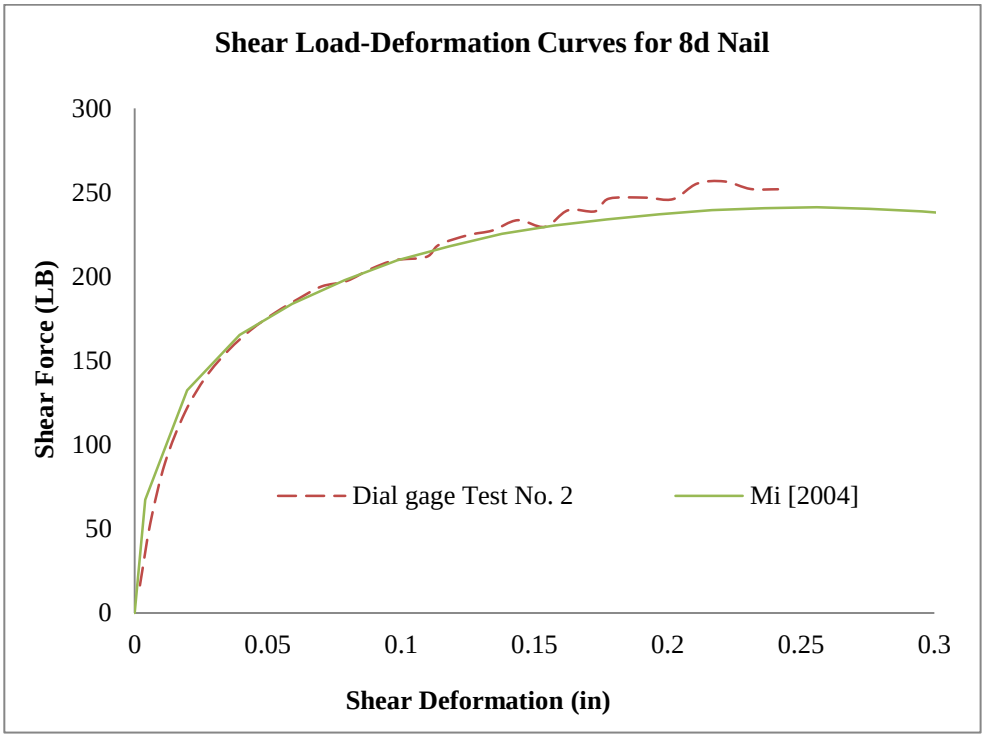

Figure 12. Shear load-deformation of one nail comparison.

4. LARGE-SCALE ROOF STRUCTURE TESTING

4.1. Testing apparatus and methods

The research team conducted all laboratory testing at the University of New Mexico's Centennial Engineering Structures Laboratory. This laboratory allowed for adequate floor space for the testing, a wide variety of testing equipment, and graduate-student assistance.

4.1.1. Testing Method

The team used air bladders to apply a uniform load across the full footprint of each scaled roof structure tested, as shown in Figure 13. Tests were performed on inverted test specimens. That is, the roof assembly's OSB surface faced the ground, while the joists were on top. The air bladder was placed between the ground and the assembly's OSB surface. As the roof assembly overlies the air bladder, a reaction header was placed on each end of the assembly to prevent the ends from displacing vertically, therefore acting in the same way as a bearing wall supports a roof. By allowing the air bladder to react against the ground, a uniformly distributed load equal to the air pressure in the bladder was applied to the inverted roof panel.

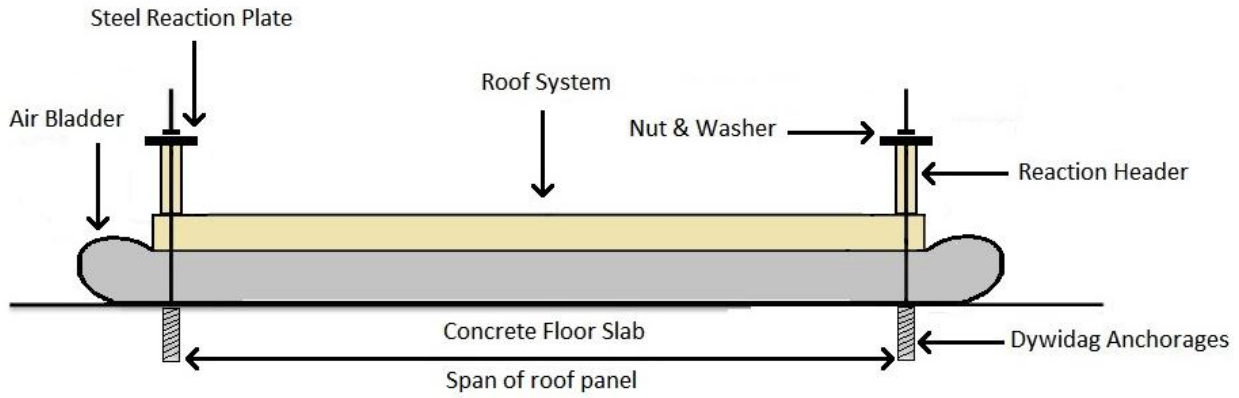

Figure 13. Side view schematic of laboratory testing (not to scale).

4.1.2. Materials

The construction of each roof assembly utilized five joists spaced at 2' on-center; the ends of each joist were then attached to like-sized end plates to complete a rigid frame (Figure 14). Once a roof frame was constructed, the frame was overlaid with 7/16" OSB decking as prescribed by the IRC (2009). The decking was then spaced 1/8" apart and nailed to the joist at 12" on-center with 8d nails. All nails used in the assembly were collated 8d galvanized coated, clipped head nails, and were driven with a pneumatic framing nail gun. Air pressure in the nail gun was set to ensure nail heads were flush with the OSB surface.

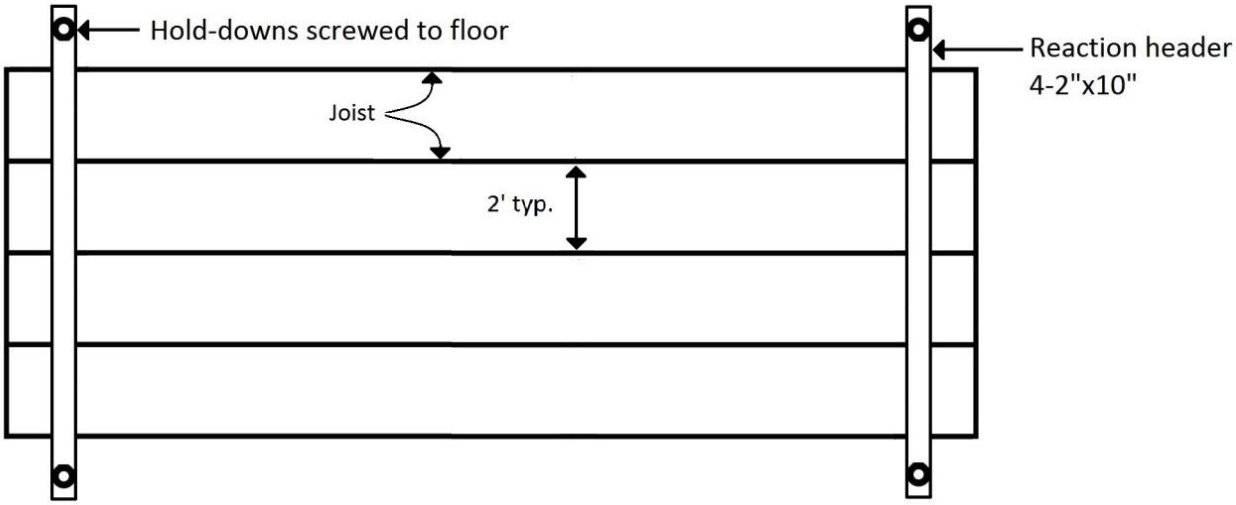

Figure 14. Schematic of laboratory test.

In preparation for a test, the completed assembly was inverted and set on top of the air bladder. The reaction headers were then placed above the assembly. All dimensional lumber and OSB decking was purchased from a local lumber retailer (Home Depot). Figure 15 provides a photograph of a roof assembly under load.

Figure 15. Photograph of roof assembly under load.

Air bladders were custom built for each test assembly plan area using 40 mil polyvinyl chloride (PVC) sheets glued together with PVC adhesive. Figures 16 and 17 show photographs of two of the PVC air bladders used.

Figure 16. Photograph of the 10'×16' PVC air bladder.

Figure 17. Photograph of the 8'×10' PVC air bladder.

4.1.3. Data Acquisition

Both manual and automated digital data-collection systems were used to measure pressure and displacement at the test assembly center. Real-time digital data acquisition was accomplished using a National Instruments eDaq in conjunction with LabVIEW software. Pressure

measurements were gathered with a Honeywell pressure transducer, while displacement was monitored through the use of a Firstmark Controls yo-yo potentiometer. Figure 18 provides a photograph of the digital data-collection system.

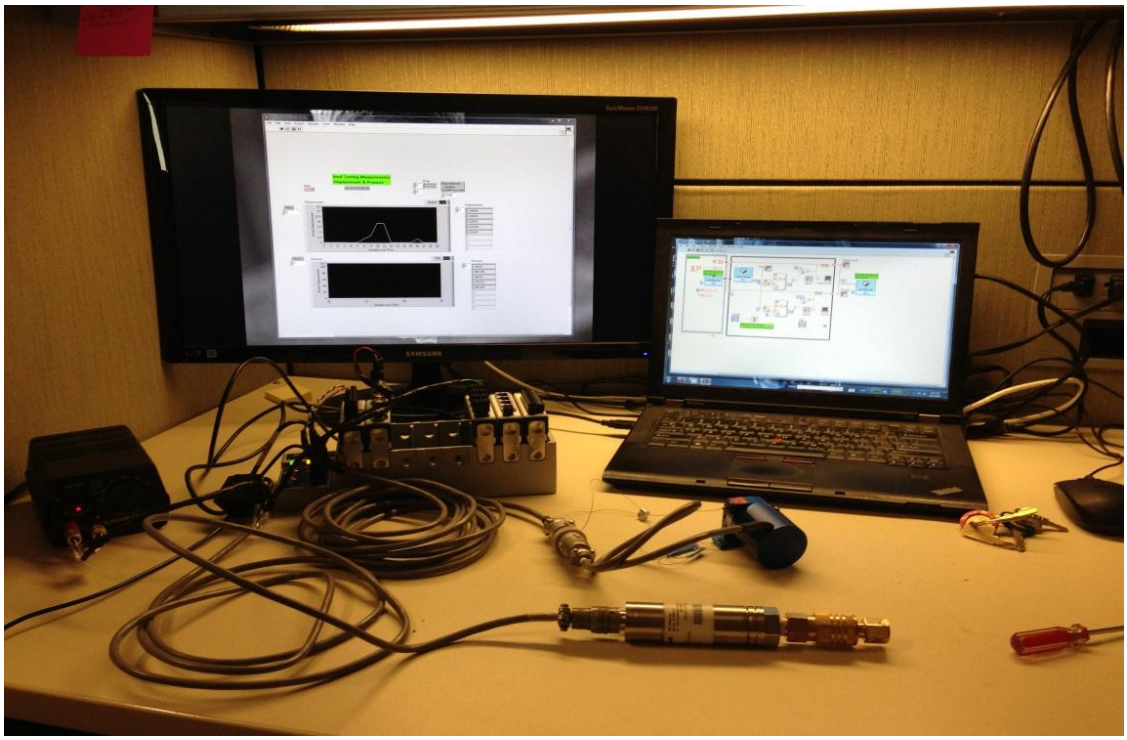

Figure 18. Digital data-collection system.

During air bladder inflation, pressure was monitored using water column manometers as shown in Figures 19 and 20.

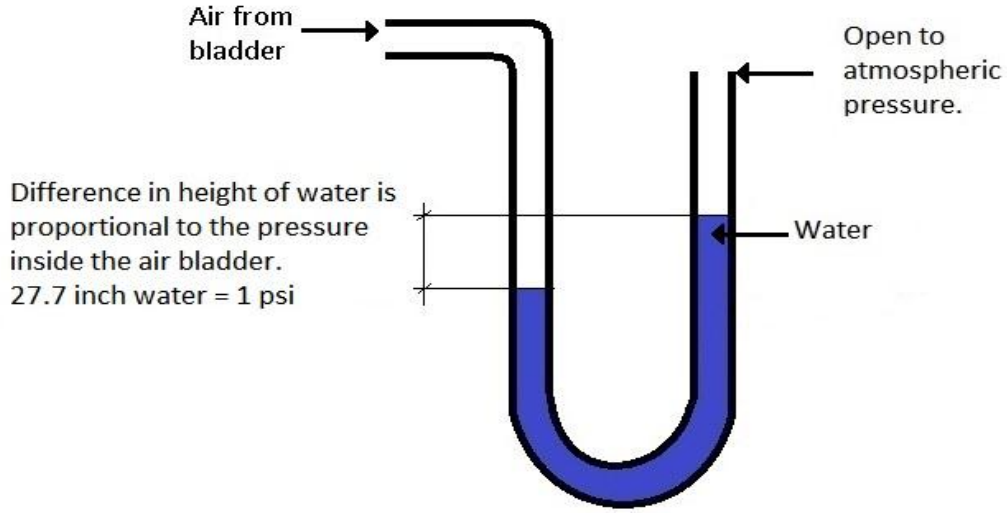

Figure 19. Manometer.

Figure 20. Photograph of double manometer used in laboratory.

During assembly testing, deflection and pressure were monitored as a function of time. Due to the loading configuration, the center of each span experienced the largest deflection. A graphical user interface was built with LabVIEW to monitor the data in real time allowing for both data logging and real-time results verification. A Fluke 189 data-logging multimeter was also used to add a layer of redundancy to the data acquisition from the pressure transducer. It is of interest to note that a multimeter can be used to monitor and subsequently record the change in voltage of a transducer; this change in voltage can then be converted to a change in pressure or position through appropriate calibration procedures. The multimeter was set to acquire a measurement every five seconds. The results were then converted to a pressure measurement and compared to the measurements made by the National Instruments eDaq system. Data collected from the two instruments were nearly identical providing added confidence to the data-acquisition accuracy. Figures 21 and 22 show the graphical user-interface and underlying LabVIEW data-acquisition program.

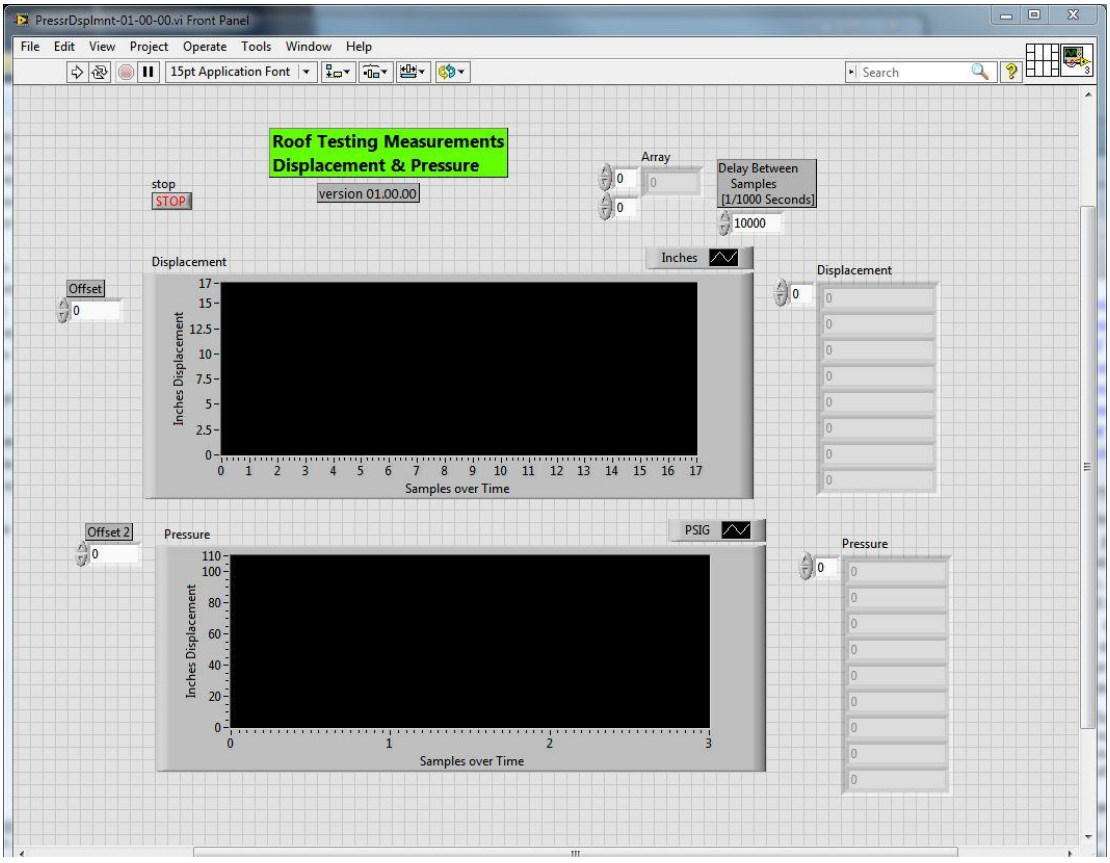

Figure 21. Real-time testing display data.

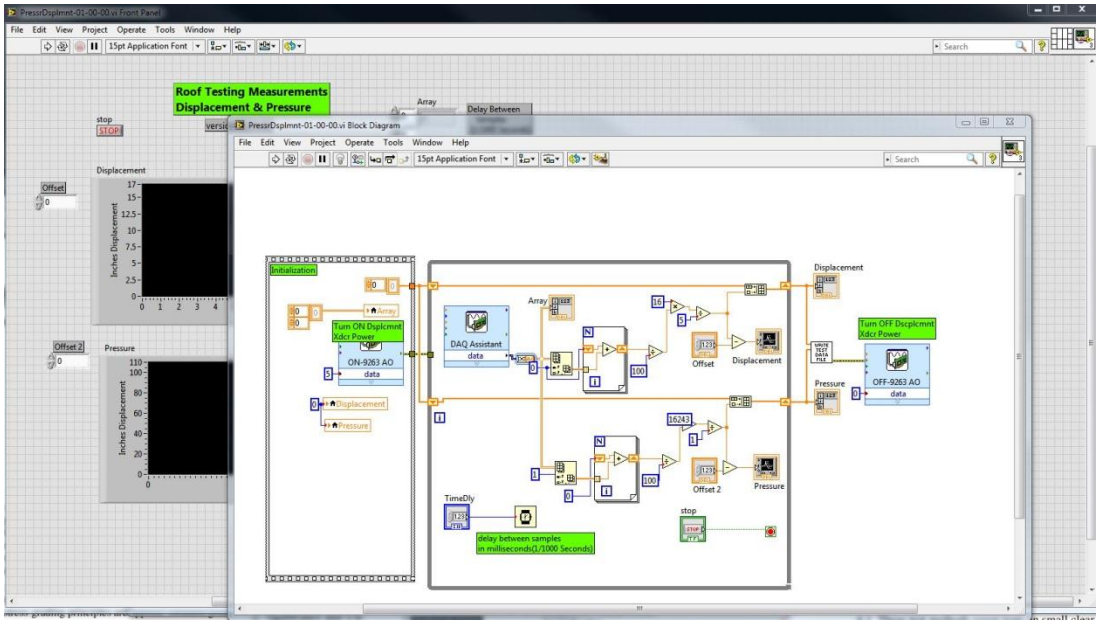

Figure 22. LabVIEW program used in data acquisition.

4.1.4. Testing Procedure

For each test, reaction headers were set at the appropriate distance to accommodate the chosen span. After the reaction headers were in place, the assembled inverted roof panel was moved, using rolling dollies, into testing position above the bladder and below the reaction headers. Next, the test assembly was clamped to the headers suspending it above the bladder to allow for perfect bladder inflation. Figure 23 is a photograph of an assembly being rolled under the reaction headers.

Figure 23. Photograph of assembly being rolled onto air bladder.

As the air bladder is inflated, the ends of the roof assembly are pushed against the reaction headers while the center portion of the roof assembly is free to deflect upwards. Once the air bladder is sufficiently inflated to support the reaction headers' full weight, the clamps used to raise and temporarily support the assembly are removed. Air bladder inflation control is accomplished using a ball valve, directly connected to a laboratory air compressor. Air flow is adjusted throughout the test to keep the air pressure constant among all air bladders. The loading rate was approximately 10 psf per minute. As pressure increased, the test roof panels deflected upward with the maximum deflection typically occurring in the assembly's center, at the center joist. During testing and as the first structural member experienced a failure, such as a crack in a joist, the pressure drops in response to the sudden increase in bladder volume.

4.2. Test results

4.2.1. Rafters

The research team tested several rafter size and span lengths (see Table 1). We conducted six separate tests of each roof-assembly category given in the table, for a total of 36 tests. Each cross section of the rafter listed is its nominal size. For example, a 2"×4" stud is really 1.5"×3.5" in actual cross sectional area.

Table 1. Tested Rafters (6 each)

Rafter Cross Section	Rafter Span
2"×4"	6'
2"×6"	14'
2"×8"	14'
2"×10"	18'
2"×12"	20'

A typical failure load curve can be seen in Figure 24. Failure of the first structural member allows for a decrease in pressure and thus identifies failure for the test assembly. It can be seen however, that failure of the initial structural member does not necessarily constitute system failure. The roof assembly generally would allow for pressure buildup well beyond the initial failure point. The team generally stopped a test when the deflection became too large for the test apparatus.

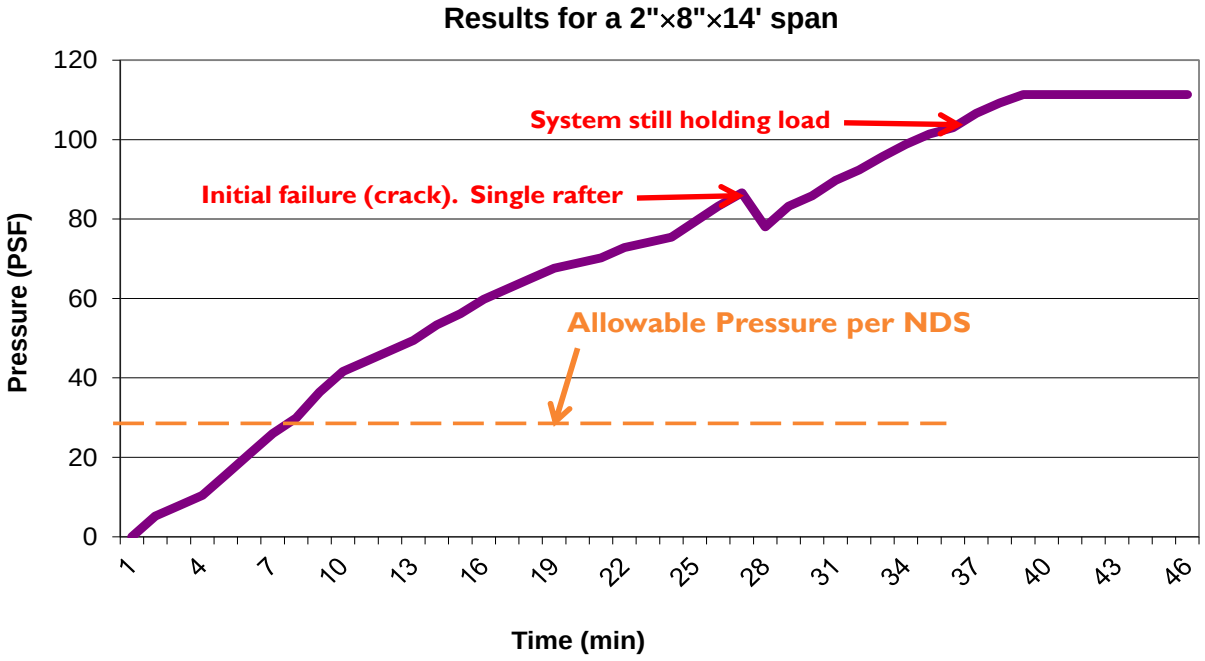

Figure 24. Typical failure curve for roof assembly.

Typical member failures during testing are shown in Figures 25 and 26.

Figure 25. Typical failure in rafter, most occurred in center.

Figure 26. Failure in rafter, some occurred in side rafters.

The rafters, purchased from a local Home Depot, were Douglas Fir-Larch. The bending design value for this material is 875 psi (National Design Specification [NDS] 2012 for No. 2 stud quality). This bending value can be adjusted for repetitive member factor (system effect) and a size factor the specific rafter used. Therefore, the adjusted design value is:

$$F_b' = F_b * C_r * C_F$$

Where:

F_b = design bending value per NDS = 875 psi

C_r = repetitive use factor = 1.15 (for members 2" to 4" thick)

C_F = size factor as listed in the NDS 2012

Therefore, the adjusted design values for the rafters tested are as shown in Table 2.

Table 2. Adjusted Design Bending Value for Rafters

Rafter	Size Factor (C_F)	Adjusted Design Bending Value (F_b')
2"×4"	1.5	1509
2"×6"	1.3	1308
2"×8"	1.2	1208
2"×10"	1.1	1107
2"×12"	1.0	1006

Table 3 presents a summary of the failure pressures for each rafter reinforced test performed.

Table 3. Summary of Rafter Supported Roof Test Results

Test No.	2"×4"	2"×6"	2"×8"	2"×10"	2"×12"
Test 1	5360	6037	4980	3030	3944
Test 2	3103	4372	2839	2546	2844
Test 3	3682	4456	2979	3150	3804
Test 4	4769	5423	3491	3490	3750
Test 5	5150	5265	4862	3560	3950
Test 6	5200	5399	3724	3315	4010

The computed average factor of safety for all rafter-based tests performed was 3.3, which means there is a 330% excess of load-bearing capacity compared to the code-defined value computed based on the NDS. Table 4 presents the computed factor of safety (FS) for each test performed

as well as the maximum and minimum factor of safety for each series of tests based on rafter size, including the series standard deviation and average.

Table 4. Factors of Safety of Rafter Supported Roof Test Results

Test No.	2"×4"	2"×6"	2"×8"	2"×10"	2"×12"
Test 1	3.6	4.6	4.1	2.7	3.9
Test 2	2.1	3.3	2.4	2.3	2.8
Test 3	2.4	3.4	2.5	2.8	3.8
Test 4	3.2	4.1	2.9	3.2	3.7
Test 5	3.4	4.0	4.0	3.2	3.9
Test 6	3.4	4.1	3.1	3.0	4.0
FS, min	2.1	3.3	2.4	2.3	2.8
FS, max	3.6	4.6	4.1	3.2	4.0
Standard deviation	0.62	0.49	0.76	0.33	0.44
Average	3.01	3.94	3.16	2.87	3.69
Median	3.29	4.08	2.99	2.92	3.85

4.2.2. Trusses

The team also tested open- and closed-web trusses. A significant difference in loading failure of truss-reinforced roof test structures compared to rafter-reinforced roof test structures is that the initial failure occurred at the system's maximum load-carrying capacity. That is, immediately after the first structural member failure in a truss-reinforced system occurred, the entire system experienced an immediate and permanent load-carrying capacity loss.

4.2.2.1. Open-Web Trusses

Failure in open-web trusses occurred in truss members (Figure 27) as well as joint connections (Figure 28). Failure produced an immediate, system-wide, permanent loss in load-carrying capacity.

Figure 27. Failure in open web (web member) truss roof test assembly.

Figure 28. Failure in open web (member connection) truss roof test assembly.

The specific trusses tested were designed for a uniform load of 40 psf based on a 2' truss spacing. The team conducted six repetitive tests of this roof assembly utilizing this specific truss design. Table 5 presents a summary the six tests performed. The average factor of safety for this series of tests was 4.0. The standard deviation was 0.2, while the median was also 4.0.

Table 5. Results of Open-Web-Supported Roof Tests

Test No.	Failure Pressure (psf)	Design Allowable Pressure (psf)	Factor of Safety
Test 1	158	40	3.9
Test 2	162	40	4.0
Test 3	175	40	4.4
Test 4	156	40	3.9
Test 5	160	40	4.0
Test 6	155	40	3.9

4.2.2.2. Closed-Web Trusses

Trus Joist (TJI) is the company that developed the wooden I-joist 50 years ago. The product is a fabricated wooden joist engineered to provide strength and stability. The I-joist is lightweight and available in long span lengths. A series of tests featuring TJIs were performed similar to the dimensional lumber testing. The failure mode was very consistent in that the top chord generally failed first. Furthermore, the beam strength is very consistent (Table 5). During several of the tests the top chord of multiple TJIs failed simultaneously (Figure 29).

Figure 29. Failure in TJI roof test assembly.

The specific TJIs tested were designed for a uniform load of 30 psf based on a 2' center-to-center truss spacing. The team conducted six repetitive tests of this roof assembly utilizing this specific truss design. Table 6 presents a summary the six test results. The average factor of safety for

this series of tests was 2.9. The standard deviation was less than 0.1, while the median was also 2.9.

Table 6. Results of TJI-Supported Roof Tests

Truss	Failure Pressure (psf)	Design Allowable Pressure (psf)	Factor of Safety
Test 1	87.5	30	2.9
Test 2	88.9	30	3.0
Test 3	84.9	30	2.8
Test 4	90.9	30	3.0
Test 5	91.2	30	3.0
Test 6	85.9	30	2.9

5. CONCLUSIONS

For all sample configurations tested, our empirical testing results indicate a greater ultimate capacity than the prescribed allowable capacity. This conclusion provides evidence that the factor of safety may be sufficiently high to offset any additional loading that occurs due to installing PV arrays.

The test results provide proof that a roof's strength is increased by system affects. The computed factors of safety further reveal that the system effects are significantly greater than the 15% allowed by the NDS.

The typical analysis methodology chosen by structural engineers nationwide to evaluate a given roof structure is to analyze a single beam or truss and extrapolate that strength across the roof. The engineer will assess the prescribed loading on the roof based on the national structural engineering code (ASCE 7-10) and apply the designated loads at the geographically suggested rate (Figure 30).

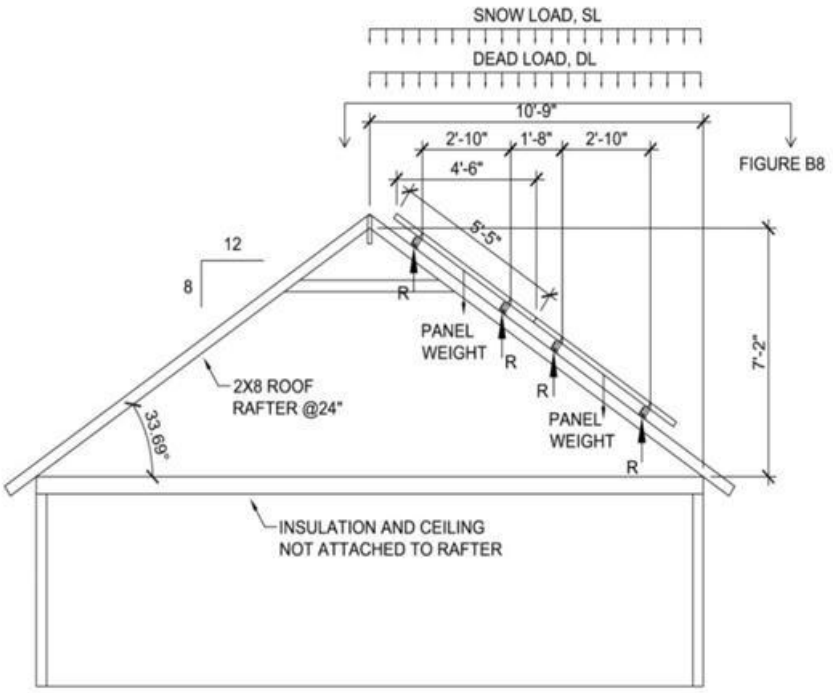

Figure 30. Example of loads applied to rooftop per ASCE 7-10.

The engineer will then apply them in combination again as suggested by the ASCE 7-10 to compute the maximum loading condition that would govern the specific project.

Load combinations utilized by the allowable stress design methodology to calculate load on roof based on geographic setting:

1. $D + F$
2. $D + H + F + L + T$
3. $D + H + F + (L_r \text{ or } S \text{ or } R)$
4. $D + H + F + 0.75(L + T) + 0.75(L_r \text{ or } S \text{ or } R)$
5. $D + H + F + (W \text{ or } 0.7E)$
6. $D + H + F + (W \text{ or } 0.7E) + 0.75L + (L_r \text{ or } S \text{ or } R)$
7. $0.6D + W + H$
8. $0.6D + 0.7E + H$

where:

D = dead load
E = earthquake load
F = load due to fluids with well-defined pressures and maximum heights
H = load due to lateral earth pressure, groundwater pressure, or pressure of bulk materials (generally zero for roof applications)
L = live load
L_r = roof live load
R = rain load
S = snow load
T = self-straining force (generally zero for roof applications)
W = wind load

Figure 31. Typical load combinations per ASCE 7-10.

The engineer would then compute the maximum bending and shear stress for the structural elements under evaluation. Thus, the actual added strength gained by a roof system is not taken into account in a typical engineer's analysis to compute an allowable stress for the structural member. If the allowable load is greater than the computed actual load, the roof strength is adequate, if not the roof has inadequate load-carrying capacity.

The difficulty and ultimately the conservatism in this approach are warranted by an engineer performing the analysis due to time and funding constraints on the project. That is, the engineer must make very conservative assumptions to enable a 'quick and dirty' analysis to meet the customer's funding constraints. However, the problem is not a simple determinate beam analysis, but a very complex nonlinear, indeterminate analysis with a material (wood) that has very conservative allowable design values applied to it.

The results from these series of tests suggest that a well-built home meeting local building standards—that has not been adversely modified or damaged—likely has adequate load-bearing capacity to support a roof-mounted PV system.

6. DISCUSSION

It is important to note that the testing performed and described in this report was completed within a set budget and time-scale and thus produced a limited number of results. However, according to the American Society of Testing and Materials (ASTM) standard 2915, a minimum of 28 tests on each joist size and type should be conducted in order to gain enough data to be representative of a sample population. Therefore, inferences concerning the FS drawn from the current research should be used with caution.

The building codes' designated allowable strength of dimensional lumber is higher if the lumber was used in a roof assembly. The increase in allowable strength is attributed to system effects that occur when more than four joists are fastened to other elements to form a composite section and is currently a 15% increase to the standard allowable values of dimensional lumber. The source of this additional capacity is found in ASTM standard 6555 *Evaluating System Effects in Repetitive-Member Wood Assemblies*. This standard has established guidelines for testing the effect of a system and has additional language that suggests the 15% increase in capacity is a conservative estimate.

Furthermore this guideline indicates that in order to allow any detectable increase in capacity the number of tests conducted must be large enough to be representative of the population as referenced in ASTM 2915. ASTM 6555 also attributes the 15% increase to capacity to three main effects: (1) load sharing (2) composite action, and (3) residual capacity of the assembly. While ASTM recognizes all three of these effects, it admittedly does not fully quantify the contribution to capacity each effect has on a system. Due to this irresolute dialogue on the part of ASTM, it becomes important to further explore ASTM 6555 as an avenue to justify nonengineered PV installations.

Load Sharing. During testing, the team observed that variations in grain pattern and knot distribution, known as coefficient of variation (COV), greatly differentiated the capacity of individual joists. Joists that had grain irregularities tended to fail before joists that were clear of incursions. When joists in the system exhibit a higher degree of COV, the load-sharing effect of the roof system increases. In other words, members that have more variation in grain and knot patterns, i.e., higher COV, cause load-sharing to increase due to the fact that such members' high COV will deflect more than members that are low in incursions, low COV, thus more load is shared.

Composite action. A common practice within the commercial construction industry is to integrate structural steel joist and poured concrete floors to achieve composite action between the joist and the flooring. When a floor is loaded, the floor transfers load to an individual joist, the transfer of load between floor and joist creates slip between the two elements. If the slip that occurs under design loads is completely prevented, then full composite action is said to exist. However, if the slip that occurs under design loads is only partially prevented, then partial composite action is said to exist. In order to achieve composite action between steel joist and concrete floor systems, the shear flow that exists between the two surfaces must be prevented by installing shear tabs. These shear tabs carry the shear flow between the concrete deck and the steel joist allowing for two individual members to act as a composite section. The composite sections that are created are both stronger and more cost effective, making composite action a relied upon design tool for structural engineers.

Although typical residential roof construction does not rely upon composite action to carry design loads, it does share the potential for increased capacity due to composite action. Partial composite action was shown to exist (Section 3) in a typical wood roof assembly, and its contribution to capacity is partially recognized, although not specifically quantified, in ASTM 6555.

7. REFERENCES

1. ASCE 7-10 (2010). Minimum Design Loads for Buildings and Other Structures. American Society of Civil Engineers. Structural engineering Institute.
2. Dwyer, S. 2012. Structural Design and Permitting for Solar Rooftop Installations. Conf, proc.: American Society of Solar Engineers annual conference, Denver, CO.
3. ASTM (n.d.). Annual Book of ASTM Standards, Volume 04.10. Sub-committee:D07. West Conshohocken, PA: ASTM International.
4. International Building Code (2009). IBC Manual. International Code Council. Country Club Hills, IL: International Code Council, Inc.
5. International Code Council (2013). Code, Standards & Guidelines. Retrieved from: http://www.iccsafe.org/Pages/default.aspx
6. International Residential Code (2009). IRC Manual. International Code Council. Country Club Hills, IL: International Code Council, Inc.
7. Mi, H. (2004). "Behavior of unblocked wood shearwalls". MScFE thesis. University of New Brunswick, Fredericton, NB.
8. National Design Standards (2012). ASD/LRFD Manual for Engineered Wood Construction. Leesburg, VA: American Wood Council.
9. Verrill, S. & Kretchmann, D.E. (2009). Material Variability and Repetitive Member Allowable Property Adjustments in Forest Products Engineering. Forest Products Laboratory: General Technical Report FPL-RP-649.

DISTRIBUTION

1 US DOE Elaine Ulrich EE-2A (electronic copy)
Building LENF950
U.S. Department of Energy
1000 Independence Avenue, SW
Washington, DC, 20585
elaine.ulrich@ee.doe.gov

1 US DOE Christina Nichols EE-3D (electronic copy)
Building LENF950
U.S. Department of Energy
1000 Independence Avenue, SW
Washington, DC, 20585
christina.nichols@ee.doe.gov

1	MS0706	Stephen F. Dwyer	6912 (electronic copy)
1	MS0706	Brian P. Dwyer	6912 (electronic copy)
1	MS1137	Geoffrey T. Klise	6926 (electronic copy)
1	MS0899	Technical Library	9536 (electronic copy)


Sandia National Laboratories